Biomechanics and Modeling in Mechanobiology (2022) 21:1325–1337
https://doi.org/10.1007/s10237-022-01590-5

ORIGINAL PAPER

Modeling and experimental investigation of electromechanical properties of scleral tissue; a CEM model using an anisotropic hyperelastic constitutive relation

Hamed Hatami-Marbini[1] · **Jafar Arash Mehr**[1]

Received: 6 December 2021 / Accepted: 1 May 2022 / Published online: 12 August 2022

Abstract
The sclera is a soft tissue primarily consisting of collagen fibers, elastin, and proteoglycans. The proteoglycans are composed of a core protein and negatively charged glycosaminoglycan side chains. The fixed electric charges inside the scleral extracellular matrix play a key role in its swelling and are expected to cause the tissue to deform in response to an electric field. However, the electroactive response of the sclera has not yet been investigated. The present work experimentally demonstrates that sclera behaves similar to an anionic electrosensitive hydrogel and develops a chemo-electro-mechanical (CEM) mathematical framework for its electromechanical response. In the numerical model, a hyperelastic constitutive law with distributed collagen fibers is used to capture the nonlinear mechanical properties of the sclera, and the coupled Poisson–Nernst–Planck equations represent the distribution of mobile ions throughout the domain. After calibrating the proposed numerical CEM model against the experimental measurements, we employ it to investigate the effects of different parameters on the scleral electromechanical response including the voltage and fixed charge density. The experimental and numerical findings of the present study confirm that sclera behaves as an electroactive hydrogel and provide new insight into the mechanical response of this ocular tissue.

Keywords Chemo-electro-mechanical model · Finite element analysis · Electrical stimulation · Sclera · Polyelectrolyte · Experiments

1 Introduction

The sclera, the opaque outer layer of the eye, is a tough fibrous tissue extending from the cornea in the front to the optic nerve head at the back of the eye. The sclera is a structurally complex connective tissue with critical roles for proper vision. It is mainly composed of collagen, proteoglycans (PGs), and elastin (Boote et al. 2020; Meek 2008). Collagen is the main structural component of scleral extracellular matrix and is responsible for its high resiliency and mechanical properties. The collagen fibers, mainly type I, are embedded in a hydrated proteoglycan network. The high tensile stiffness of collagen fibers and the relatively low stiffness of the interfibrillar proteoglycan matrix primarily define the mechanical response of sclera. The proteoglycans are attached to collagen fibers via their core proteins, while their glycosaminoglycan (GAG) side chains behave as bridges between neighboring collagen fibers (Cheng et al. 2013; Hatami-Marbini and Pinsky 2009; Lewis et al. 2010; Scott and Thomlinson 1998). GAGs can be divided into two main groups of non-sulfated and sulfated GAGs. The chondroitin sulfate (CS), dermatan sulfate (DS), keratan sulfate (KS), and heparin sulfate (HS) are among the commonly seen sulfated GAGs (Gandhi and Mancera 2008; Pomin and Mulloy 2018). These sulfated GAGs are negatively charged with a strong tendency to attract and retain large volume of water molecules into the scleral extracellular matrix. In addition to the importance of GAGs in fibrillogenesis (Chen et al. 2020; Chen and Birk 2013; Vogel and Trotter 1987), they play important roles in hydration and mechanical properties of ocular tissues (Hatami-Marbini 2014; Hatami-Marbini and Etebu 2013; Hatami-Marbini et al. 2013; Hatami-Marbini and Pachenari 2020a, b, c; Pachenari and

✉ Hamed Hatami-Marbini
hatami@uic.edu

[1] Mechanical and Industrial Engineering Department, University of Illinois at Chicago, 2039 Engineering Research Facility, 842 West Taylor St, Chicago, IL 60607, USA

Hatami-Marbini 2021; Rada et al. 1997). The GAG repeating units, called disaccharides, are composed of an uronic acid and an amino sugar (Zhang et al. 2010). At physiological pH, GAGs are negatively charged because of deprotonation of their carboxylic acid and sulfate groups. Collagen molecules also contain electric charges at non-physiological pH; however, their net electric charge is almost zero at physiological pH, i.e., the total net negative charge of the sclera at neutral pH is because of the GAGs. The scleral extracellular matrix can be considered as an electroactive polyelectrolyte in which GAGs with a net electrical charge are chemically bound to collagen fibers (Elliott and Hodson 1998; Huang and Meek 1999; Loret and Simões 2010).

The primary objective of the present study was to characterize the electromechanical response of the scleral tissue using an experimental and numerical framework. For this purpose, we used an experimental technique that has commonly been used to investigate the mechanical response of electroactive hydrogels under an applied electric potential (Bassil et al. 2011; Li et al. 2016; Morales et al. 2014; Shang et al. 2008a, b; Shiga and Kurauchi 1990; Sun and Mak 2001; Yew et al. 2007; Zhang et al. 2020). In this approach, rectangular-shaped hydrogel strips are placed between two parallel carbon electrodes in a chamber filled with solution and their deformation is measured after applying the electric potential. The applied DC electric field exerts an effective force on the charges inside the gels and solution. Furthermore, the external electric field causes unbalanced local swelling of hydrogel strips leading to their bending in response to the applied electric field (Doi et al. 1992; Gong et al. 1994). The extracellular matrix of sclera includes immobile GAGs that are negatively charged; thus, it is expected that when it is placed between two electrodes in a salt solution, it shows the same bending response that has been documented for electroactive hydrogels. We tested this hypothesis in the present work and characterized the parameters that affect the mechanical deformation of the sclera under an external electric potential.

In addition to experimentally investigate the electroactive response of the scleral tissue, we developed a chemo-electro-mechanical mathematical framework and numerically described the experimental measurements. In the following, a brief overview of the previous numerical modeling of polyelectrolyte gels is given; refer to (Chinthala et al. 2021; Wallmersperger et al. 2013) for more complete review. Flory and Rehner were among the first who presented a statistical theory for swelling of charged network structures based on the entropy change (Flory and Rehner 1943a, b). This macroscopic theory works well for chemical stimulations where the concentration of ion species is independent of their spatial position. However, it becomes cumbersome when ion concentrations are dependent on their local position in the gel, for example, in the presence of an electric field (Guelch et al. 2000). Thus, coupled multi-field formulations have been created to express the coupling between electrical, chemical, and mechanical fields governing the behavior of polyelectrolyte hydrogels (Ballhause and Wallmersperger 2008; De Gennes et al. 2000; De et al. 2002; De and Aluru 2004; Grimshaw et al. 1990; Wallmersperger et al. 2004, 2007). In coupled multi-field formulations, chemical and electrical field equations are used to numerically represent the distribution of ion concentration and electric potential, while mechanical field equations give the deformation of gels. The osmotic pressure, defined based on ion concentration differences, is used to couple different equations together. The chemo-electro-mechanical (CEM) multi-field equations have been solved using different methods for different purposes in the literature (Ballhause and Wallmersperger 2008; De et al. 2002; De and Aluru 2004; Li and Lai 2011; Wallmersperger et al. 2004; Yew et al. 2007). For example, the large deformation electromechanical response of ionic hydrogels was numerically examined by a CEM model based on higher-order terms in the strain tensor and a linear elastic constitutive model (Elshaer and Moussa 2014). The bending behavior of electrically stimulated cantilevered hydrogels was also explored using a CEM model developed based on a linear elastic model and solved by FEM (Attaran et al. 2015, 2018). A similar model was recently used for characterizing the properties of electroactive hydrogels for possible use in cartilage-tissue repair applications (Farooqi et al. 2020). In addition to the CEM models, other models such as multi-phasic mixture theory (Hatami-Marbini 2013) can also be used to simulate the behavior of ionic gels (Li et al. 2004; Yuan and Li 2013). In the present study, we developed a novel nonlinear CEM formulation that uses an anisotropic nonlinear hyperelastic material model for the mechanical response of the sclera and the nonlinear coupled Poisson–Nernst–Planck model for the interactions and distribution of free ion interactions and electrostatic potential. The resulting coupled nonlinear CEM equations were solved using the finite element method in order to numerically represent experimental measurements and investigate the effect of various parameters on the electroactive response of the sclera.

2 Materials and methods

2.1 Experiments

Fresh porcine eyes were collected from a slaughterhouse and were brought to the laboratory within 1 h. In the laboratory, fat and extraocular muscles were removed carefully from the eyeballs. Then, scleral strips of size 25 mm by 2.5 mm were excised in superior–inferior direction in vicinity of the equator line from each eyeball (Fig. 1a).

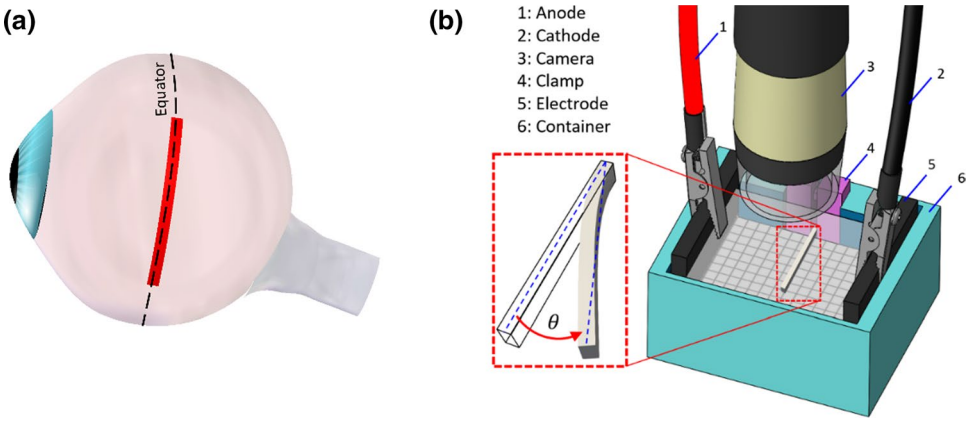

Fig. 1 **a** The scleral strips were obtained from the vicinity of the equator line in the superior–inferior direction. **b** The schematic illustration of the experimental setup. The scleral strips were immersed in 0.15 M NaCl solution and were fixed between clamps. The electric voltage was applied and a digital camera recorded the deformation of strips. The bending angle was defined as the angle that a straight line connecting the free and clamped ends of scleral strips before and after deformation

The thickness of samples was measured using an ultrasonic pachymeter (DGH 555B—Exton, PA, USA), and they were mounted into a custom-designed chamber in order to measure their mechanical response under a DC electric field.

The custom-designed chamber was made up of two electrodes, 5 cm apart, and a clamp in the middle for holding one end of the samples firmly in place. The scleral strips were placed in the testing chamber from their superior side end, i.e., all samples were clamped from the same side. The free end of the strips was marked with a small red dot of size about 1 mm in order to track the movement of their tips. The chamber was filled with 0.15 NaCl solution, and an electric potential was applied using a DC power supply (BK Precision 1666, CA, USA) for 60 s. All experiments were done at 37 °C temperature, and the temperature of the solution was monitored using a thermometer (OMEGA HH911T, CT, USA). We used an electric potential of 10, 12.5, and 15 V and tested five scleral strips at each voltage. We selected these voltages in order to induce a measurable deformation and characterize the dependence of bending deformation of sclera on voltage. However, these voltages may not be physiologically relevant.

Because of the application of the voltage, the strips were bent. The deformation of specimens was recorded using a high-resolution digital microscope (Koolertron 5MP 20-300X, Shenzhen, China) that were mounted perpendicular to the testing device (Fig. 1b). The bending angle was defined as the rotation, measured in degrees, of the line passing through the point at the clamped end of the samples and the point at their free end. A Python code using OpenCV was written to automatically extract the movement of sample tips from these recordings (Bradski and Kaehler 2008), i.e., the bending angle of scleral strips was calculated automatically and in real time. Figure 1 shows the main components of the experimental setup schematically.

The experiments were performed in NaCl solution in order to have only two mobile ion species in the bathing solution and avoid unnecessary complications in the proposed numerical model. We used a universal pH indicator (Bogen's universal pH indicator solution) to monitor the propagation of pH waves upon applying the voltage inside the custom-designed chamber filled with saline solution. These tests were used to choose the duration of electrical stimulations such that pH waves do not reach the samples and influence experimental measurements.

2.2 Numerical model

The nonlinear coupled Poisson–Nernst–Planck (PNP) system describes the concentration of charged ion species under the influence of both an ionic concentration gradient ∇c and an electric potential ϕ (Attaran et al. 2015; Ballhause and Wallmersperger 2008; Chen and Ma 2006; De and Aluru 2004; Luo et al. 2007; Wallmersperger et al. 2004),

$$\begin{aligned} \frac{\partial c_\alpha}{\partial t} &= \nabla \cdot \left(D_\alpha \nabla c_\alpha + \mu_\alpha F z_\alpha c_\alpha \nabla \phi \right), \ \alpha = \mathrm{Na}^+, \mathrm{Cl}^- \\ \nabla^2 \phi &= -\frac{F}{\varepsilon_\mathrm{r} \varepsilon_0} \sum_{\alpha = \mathrm{Na}^+, \mathrm{Cl}^-, \mathrm{fixed}} z_\alpha c_\alpha \end{aligned} \tag{1}$$

where t is the time, D_α is the diffusivity of ionic species, c_α is the concentration of species, z_α is the valence of species, $\mu_\alpha = D_\alpha / RT$ is the mobility of ionic species, F is the Faraday constant, T is the temperature, R is the gas constant, ε_0 is the electrical permittivity of vacuum, and ε_r is the relative permittivity.

The theory of linear elasticity has often been used to describe the mechanical field in previous numerical models proposed for simulation of electroactive hydrogels (Attaran et al. 2015; Ballhause and Wallmersperger 2008; Luo et al. 2007; Wallmersperger et al. 2004, Mehr and Hatami-Marbini 2022). However, the sclera has a complex nonlinear hyperelastic behavior and the orientation of collagen fibers should play a key role in defining its mechanical response. Thus, we herein used the following strain energy function, which is the summation of strain energy of the matrix $F_{\mathrm{m}}(\tilde{I}_1)$ and that of the collagen fibers $F_{\mathrm{f}}(\tilde{\lambda})$, to represent the mechanical properties of scleral tissue (Girard et al. 2009a; Hatami-Marbini and Maulik 2016; Holzapfel 2000; Wang and Hatami-Marbini 2021; Weiss et al. 1996),

$$\widetilde{W} = F_{\mathrm{m}}(\tilde{I}_1) + \int_{\alpha_p-\frac{\pi}{2}}^{\alpha_p+\frac{\pi}{2}} P(\alpha) F_{\mathrm{f}}(\tilde{\lambda}) \mathrm{d}\alpha + \frac{K}{2}(\ln J)^2 \tag{2a}$$

where

$$\begin{aligned} &F_m(\tilde{I}_1) = c_1(\tilde{I}_1 - 3) \\ &F_f(\tilde{\lambda}) = c_3\left(e^{-c_4}(Ei(c_4\tilde{\lambda}) - Ei(c_4)) - \ln\tilde{\lambda}\right) \\ &\tilde{\lambda}^2 = \tilde{I}_4 = \mathbf{a}_0(\alpha)\cdot\tilde{\mathbf{C}}\cdot\mathbf{a}_0(\alpha), \end{aligned} \tag{2b}$$

and $P(\alpha)$ is the semicircular von Mises fiber distribution function defined as,

$$P(\alpha) = \frac{1}{\pi I_0(k_f)} e^{k_{\mathrm{f}}\cos 2(\alpha-\alpha_p)}. \tag{2c}$$

In the above equations, k_{f} is the fiber concentration factor controlling the collagen fiber alignment along a preferred fiber orientation α_{p} and $I_0(k)$ is the Bessel function of the first kind,

$$I_0(k_f) = \frac{1}{\pi}\int_0^{\pi} e^{k_{\mathrm{f}}\cos x}\mathrm{d}x. \tag{2d}$$

Furthermore, $\tilde{I}_1$ and $\tilde{I}_4$ are the first and fourth invariants of the isochoric right Cauchy–Green deformation tensor $\tilde{\mathbf{C}}$, $\tilde{\lambda}$ is the deviatoric part of the stretch along the fiber direction, J is the determinant of the deformation gradient, $\mathbf{a}_0(\alpha)$ is the unit vector representing the collagen fiber direction, Ei is the exponential integral function, K is the bulk modulus, c_3 is the exponential fiber stress coefficient, and c_4 is the rate of uncrimping collagen fibers (Grytz and Meschke 2009).

The coupling of chemo-electro-mechanical fields was defined through the differential osmotic pressure $\Delta\pi$ and its relation to the body force $\mathbf{b}$ that appears in the linear momentum equation (Ballhause and Wallmersperger 2008; Bassetti et al. 2005; De and Aluru 2004; Doi et al. 1992; Shang et al. 2008b; Shiga and Kurauchi 1990; Wallmersperger et al. 2004)

$$\mathbf{b} = \nabla\left(\Delta\tilde{\pi}_1 - \Delta\tilde{\pi}_2\right) \tag{3}$$

where $\Delta\tilde{\pi}_1$ and $\Delta\tilde{\pi}_2$ are the normalized differential osmotic pressures at the anode side and cathode side, respectively. The normalized differential osmotic pressure is defined as

$$\Delta\tilde{\pi} = \frac{\Delta\pi}{RT} = \sum_{i=\mathrm{Na}^+,\mathrm{Cl}^-}\left[(c_i)_{\mathrm{sclera}} - (c_i)_{\mathrm{solution}}\right]. \tag{4}$$

After deriving the weak forms of PNP and mechanical partial differential equations, we discretized them in time using backward Euler scheme and linearized them using Newton's method (Langtangen and Mardal 2016). We then implemented them in the open-source platform FEniCs in order to solve them using the finite element method (Alnæs et al. 2015; Logg et al. 2012). Two different solution strategies have been commonly used in the literature. One could solve chemo-electrical fields at a given time step, use the results for solving the mechanical field equations, then update the geometry (based on the solution of mechanical fields), and solve chemo-electrical fields in the next time step, and keep repeating this procedure at all time steps. This method is called a fully coupled approach and is computationally expensive. In the second solution method, chemo-electrical fields are first solved to obtain the ion concentration and electric potential distribution in the sclera and surrounding solution at all time steps without updating the simulation domain geometry. Then, mechanical field equations are solved in order to obtain the deformation of the scleral region. The latter method, which we used in the present work, does not require the geometry of the simulation domain to be updated at each time step and thus is computationally less involved. This semi-coupled solution method has often been used for problems where the deformation of the solid domain is not very large.

We first validated our implementation of the fiber constitutive model, Eq. (3), in FEniCs by comparing our numerical solution of a biaxial extension test on a hexahedron element with its analytical solution (see "Appendix 1"). We also validated our implementation of the above coupled CEM model in FEniCs against a previous study (Wallmersperger et al. 2004) in which a linear elastic theory has been used (see "Appendix 2"). Figure 2 shows the geometry that was used to represent experimental measurements in our numerical simulations. In the present work, we used a 2D geometry, because of existing symmetries, for solving chemo-electrical fields and a 3D geometry, including the collagen fiber orientation, for solving mechanical equilibrium equations. The solution of the PNP system gave the chemical and electrical fields. The Lagrange elements were used, and the required mesh resolution was found such that the number of elements had no significant effect on the numerical results. The mesh density was increased significantly at the sclera–solution

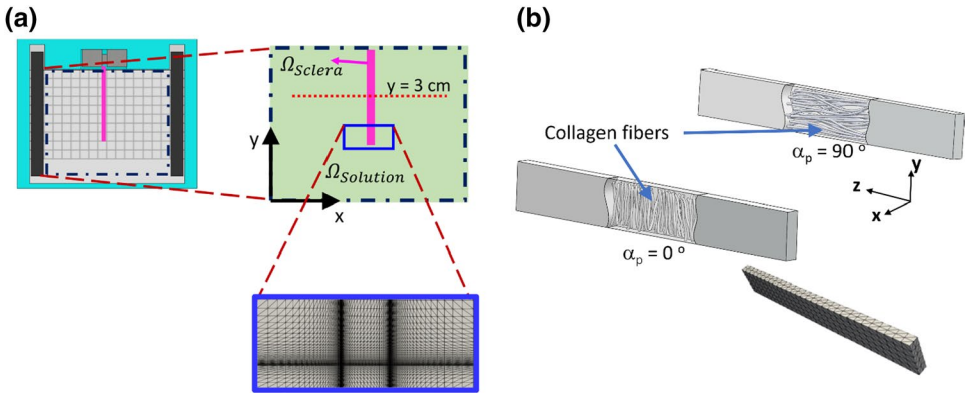

Fig. 2 **a** Schematic 2D illustration of computational domains including the solution and scleral strips. **b** Scleral strips were modeled in 3D with α_p defining the orientation of collagen fibers in the *yz*-plane: $\alpha_p = 0$ and $\alpha_p = 90°$ correspond to when collagen fibers are aligned in the *y*- and *z*-axis, respectively

interfaces in order to be able to capture the steep gradient of mobile ion concentrations at this region (Fig. 2a). The following boundary and initial conditions were used for the PNP system (chemo-electrical field). The molarity of the NaCl solution in experiments was 0.15; thus, we used $c_{Cl^-} = c_{Na^+} = 150$ mol/m^3 in the solution domain. Furthermore, half of the applied electric potential in the experiments was applied at the anode and $-\phi/2$ was applied at the cathode. The initial concentration of mobile species inside the scleral domain was obtained from the ideal Donnan equation (Gu et al. 2004; Lanir et al. 1998):

$$\begin{aligned} \left(c_{Na^+}\right)_{sclera} &= \frac{c_{fixed} + \sqrt{c_{fixed}^2 + 4\left(c_{Na^+}\right)_{solution}^2}}{2} \\ \left(c_{Cl^-}\right)_{sclera} &= \frac{-c_{fixed} + \sqrt{c_{fixed}^2 + 4\left(c_{Cl^-}\right)_{solution}^2}}{2}. \end{aligned} \tag{5}$$

Furthermore, we used $F = 96{,}487$ C/mol, $\varepsilon_0 = 8.85 \times 10^{-12}$ F/m, $\varepsilon_r = 75$, $z_{Na^+} = -z_{Cl^-} = -z_{fixed} = 1$, $R = 8.3143$ J/mol K, $T = 310$ K, $D_{Na^+} = 1.16 \times 10^{-9}$, and $D_{Cl^-} = 1.6 \times 10^{-9}$ (Gu et al. 2004; Liu et al. 2005). The mechanical field was solved by constructing a 3D bar-shaped geometry representing scleral strips with length of 20 mm, width of 2.5 mm, and thickness of 0.75 mm. We assumed collagen fibers to be distributed in the *yz*-plane. The scleral strips were clamped at the top in the experiments; thus, zero Dirichlet displacement boundary conditions were applied at the top of the scleral domain.

In order to find the material constants, i.e., fixed charge density (FCD), c_1, c_3, c_4, and k_f, we used the differential evolution optimization algorithm to find the closest numerical fit to experimentally measured bending angles (Price et al. 2006). The cost function h was defined as

$$h = \sqrt{\frac{1}{m}\sum_{i=1}^{m}\left(\overline{\theta}_{i,exp} - \overline{\theta}_{i,num}\right)^2} \tag{6}$$

where $\overline{\theta}_{i,exp}$ and $\overline{\theta}_{i,num}$ are average bending angles at time i obtained experimentally and numerically, respectively. We fitted the numerical model to the average bending angles obtained from the experiments conducted at 10 V, 12.5 V, and 15 V separately. Furthermore, we selected 10 KPa $\le c_1 \le$ 500 KPa, 5 KPa $\le c_3 \le$ 100 KPa, $50 \le c_4 \le 1000$, $0.1 \le k_f \le 10$ as model parameter ranges in the differential evolution algorithm (Feola et al. 2016; Girard et al. 2009a, b). In all numerical simulations, the bulk modulus $K = 10$ MPa was used to ensure incompressibility (changing K to higher values had very little impact).

3 Results and discussion

The average thickness of 15 scleral samples was 0.78 ± 0.03 mm which agrees with previous studies (Pachenari and Hatami-Marbini 2021). There was no significant change in the weight and thickness of samples before and after the experiments. All experiments were done at 37 °C temperature, and no significant change in the temperature was observed. The following chemical reactions at the vicinity of the electrodes occur because of the external electric field:

$$2H_2O + 2e^- \rightarrow H_2 + 2OH^- \quad \text{(Cathode)}$$
$$6H_2O \rightarrow O_2 + 4H_3O^+ + 4e^- \quad \text{(anode)}.$$

The hydroxide and hydronium ion transfer into the solution creates pH waves that propagate from each electrode with a velocity proportional to the magnitude of the external electric field (Glazer et al. 2012). The penetration of pH waves into scleral strips could affect their bending response by altering the amount of their fixed charges; however, the proposed numerical model does not include the variation of fixed charges due to the pH variation (O'Grady et al. 2009). The influence of pH gradient has previously been reported in electroactive hydrogels (Glazer et al. 2012; Kim et al. 1999; O'Grady et al. 2009; Shang et al. 2008b). The

interpretation of experimental measurements becomes difficult if the electric potential is applied long enough for the pH waves to reach scleral strips. Here, we limited the duration of the experiments such that pH waves did not influence the measured scleral deformation. For this purpose, we used the universal pH indicator (Bogen's universal pH indicator solution) and characterized the propagation of pH waves inside the solution upon applying the voltage. Figure 3 indicates that it took more than one minute for the pH waves to reach the center of the testing chamber, i.e., the location of the samples. This observation confirms that the penetration of pH waves did not affect the measured bending response of scleral strips. Figure 3 also suggests that hydroxide ions moved faster compared to hydronium ions, which agrees with previous studies (Glazer et al. 2012).

Figure 4 shows the bending angle of anterior scleral strips as a function of time as they were subjected to the electric potential. The scleral strips bent toward the cathode under an external electric field, suggesting that the sclera is an anionic polyelectrolyte. This electroactive behavior is because applying the voltage causes mobile ion species inside the domain to migrate toward their counter electrodes (Kim et al. 1999; Li et al. 2016). This ion transportation affects the concentration of sodium and chloride ions near interfaces of the sample and solution leading to generation of differential osmotic pressure at different sides of scleral strips. As the osmotic pressure near the anode side of strips was higher compared to the cathode side, they bent toward the cathode. The experimental results presented in Fig. 4 also demonstrate the effect of the voltage on the bending angle of scleral strips. Increasing the voltage from 10 to 15 V increased the average bending angle after 60 s from nearly from 4° to 9°. This is because increasing the voltage leads to higher speed of ion movement inside the solution, i.e., the faster creation of differential osmotic pressure at the interface of the solution and sample causes larger electroactive bending deformation. The dependence of the bending response on the strength of the electric potential observed here is in agreement with previous studies on polyelectrolyte hydrogels (Jiang et al. 2019; Kim et al. 1999; Li et al. 2016; Shang et al. 2008a, b).

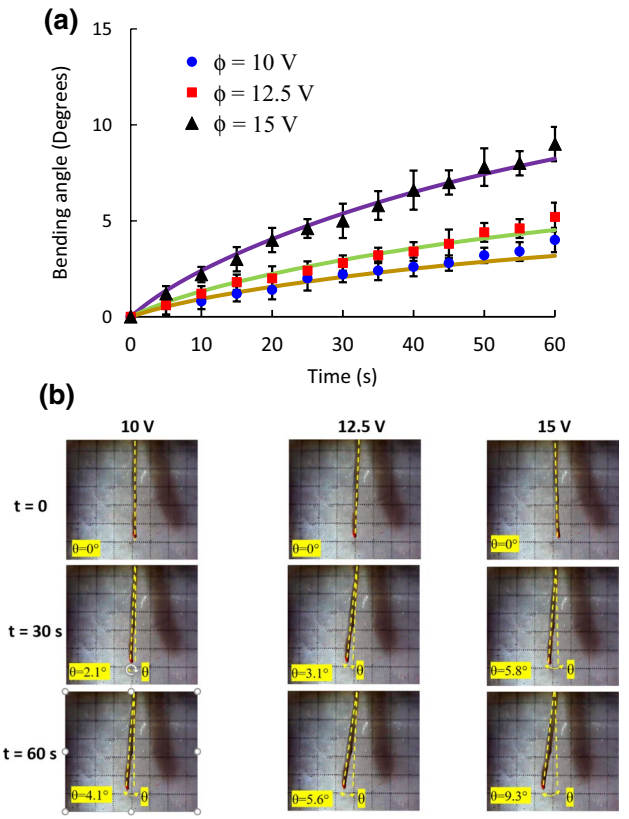

Fig. 4 **a** The effect of electric potential on the bending angle of scleral strips in 0.15 M NaCl solution. The symbols show the experimental measurements, and solid lines represent the fits obtained from the numerical model. **b** The bending of typical scleral strips at 10 V, 12.5 V, and 15 V at 0, 30 s, and 60 s

We numerically simulated the electroactive bending response of scleral strips by presenting and implementing a FEM-based CEM model. For this purpose, we solved

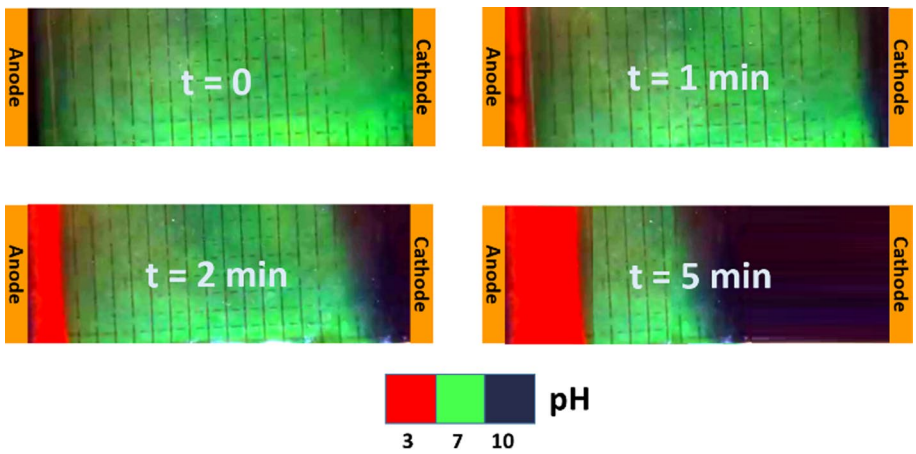

Fig. 3 Propagation of pH waves from the electrodes at 15 V in 0.15 M NaCl solution before, after 1 min, after 3 min, and after 5 min of the electrical stimulation. The green color corresponds to the neutral medium (i.e., pH ~ 7), while the red and black colors show the acidic (i.e., pH ~ 3) and basic (i.e., pH ~ 10) mediums, respectively

nonlinear coupled constitutive equations of the PNP system along with the governing equations for the mechanical field. The solid lines in Fig. 4 represent the numerical fits to experimental measurements. We determined constitutive model parameters, c_1, c_3, c_4, and k_f from fitting the numerical model to experimental measurements using the differential evolution optimization algorithm. Table 1 gives material parameters of the numerical model that was obtained. It is noted that the estimated fixed charge density (FCD), c_{fixed} ≈ 7.5–8.2 mM, is within previous reports for the expected scleral GAG content. The scleral GAG content is almost one quarter of corneal GAG charge density of 30–40 mM (Borcherding et al. 1975; Forrester et al. 1996; Huang and Meek 1999; Loret and Simões 2017).

Table 1 The model parameters that were obtained from fitting the average experimental measurements at different voltages

Parameters	Values		
	(ϕ = 10 V)	(ϕ = 12.5 V)	(ϕ = 15 V)
c_1	125.56 Kpa	107.98 Kpa	97.23 Kpa
c_3	27.86 Kpa	26.06 Kpa	24.19 Kpa
c_4	281.47	293.48	160.53
K	10 Mpa	10 Mpa	10 Mpa
k_f	3.18	2.81	2.99
α_p	0°	0°	0°
c_{fixed}	8.18 mM	7.53 mM	7.54 mM

Unless otherwise mentioned, the material parameters obtained for experiments done at ϕ = 10 V were used in parametric numerical studies investigating mobile ion distributions and effects of the FCD and collagen fibril orientations

The numerical predictions for the deformation of scleral strips and mobile ion distributions under 10 V of electrical stimulation are shown in Fig. 5a. The results shown in this plot are obtained from simulating the electroactive bending response of the sclera using the FEM-based CEM model (Table 1). The gradual forming of concentrations gradient near the interface of the sample and solution is shown in Fig. 5b. At the beginning (t = 0), the distribution of mobile ions has a step shape. Upon applying the electric voltage, the gradient of concentrations adjacent to the anode and cathode sides of the samples increases continuously with time. This time-dependent behavior of mobile ion distributions is similar to what has previously been reported in other studies (Attaran et al. 2015; Wallmersperger et al. 2004). The respective increase and decrease of ion concentrations near the cathode and anode are in agreement with the theory of depletion polarization (Kwon et al. 1994).

We investigated numerically the effect of the electric voltage and FCD on the distribution of mobile Na^+ and Cl^- ions in Fig. 6. It is noted that the gradient of mobile ion concentrations in the vertical direction is negligible because of the dimension of samples and the experimental setup. In these figures, the mobile ion concentration is plotted along x-axis (y = 0.03 m). An increase in concentrations at the boundaries of scleral strips and the solution is seen with

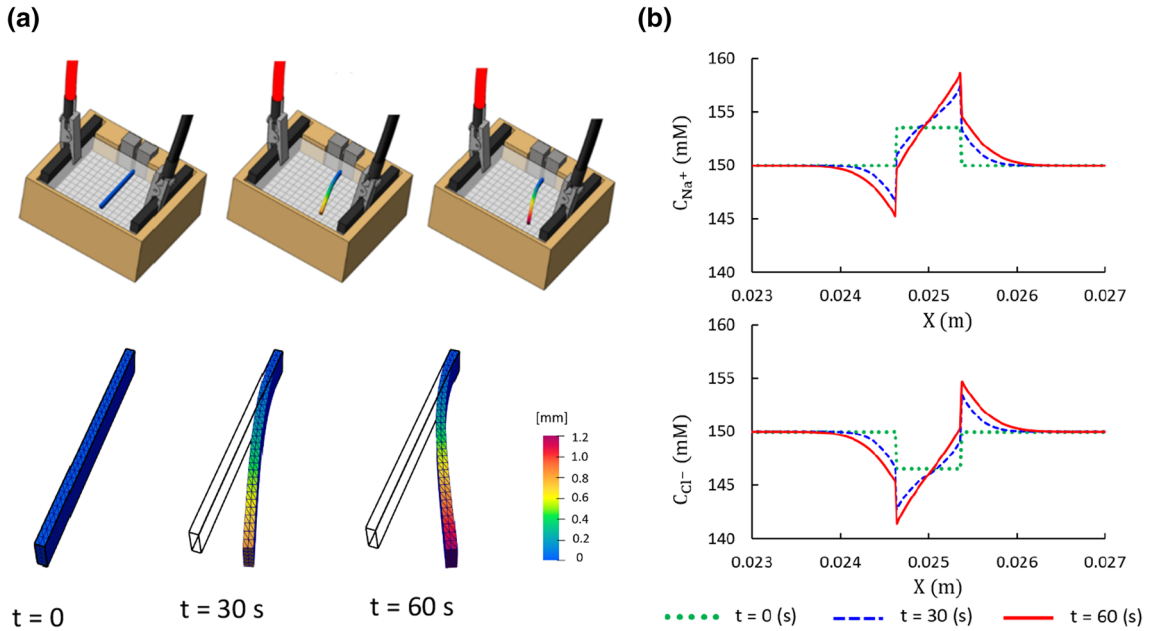

Fig. 5 **a** The numerical results for the deformation of scleral strips under 10 V at t = 0, t = 30 s and t = 60. The deformations are presented in 3X exaggerated. The color bar represents the magnitude of displacement, and solid black lines correspond to the initial shape of the sample before applying the voltage. The black and red terminals correspond to the cathode and anode. **b** The distribution of sodium and chloride ion concentrations at y = 0.03 m under 10 V

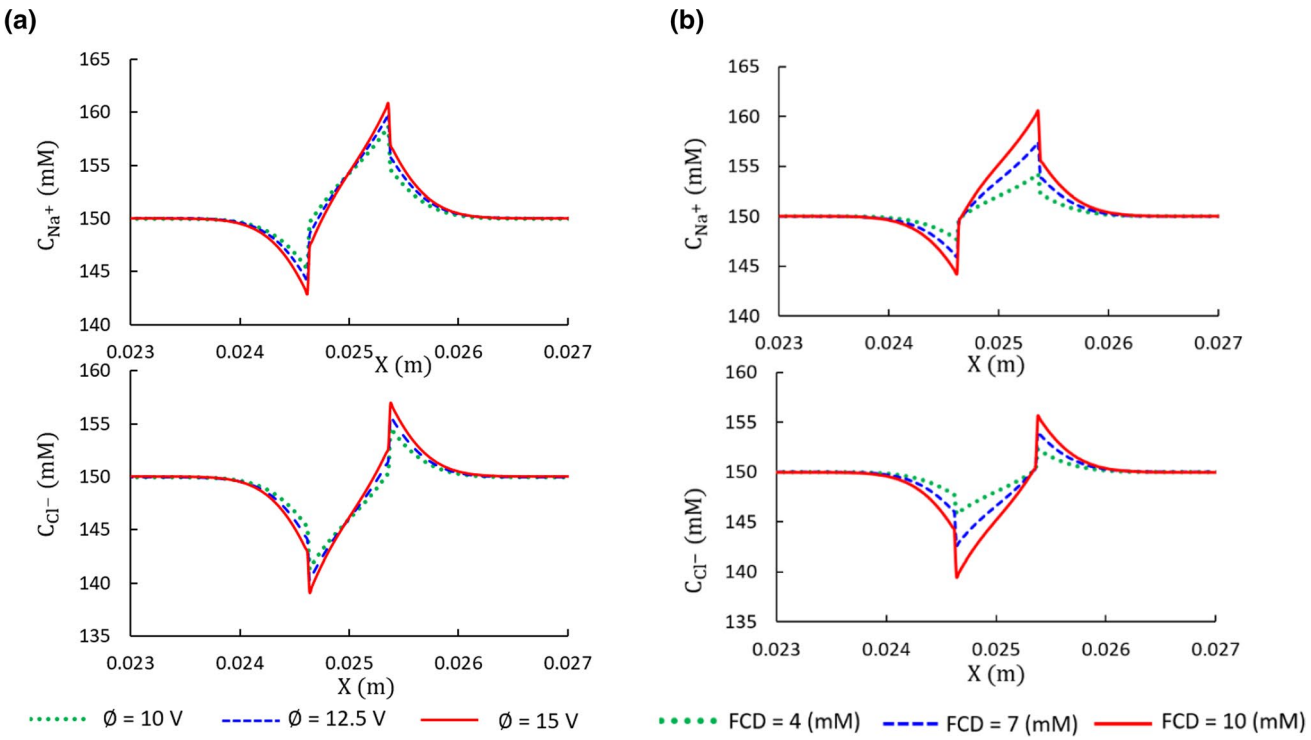

Fig. 6 **a** The effect of voltage on the concentration of sodium and chloride ions in 0.15 M NaCl solution. **b** The effect of FCD on the concentration of sodium and chloride ions. The results are obtained at $y = 0.03$ m after 60 s of electrical stimulation. The numerical simulations were done using model parameters reported in Table 1 for experiments performed at 10 V

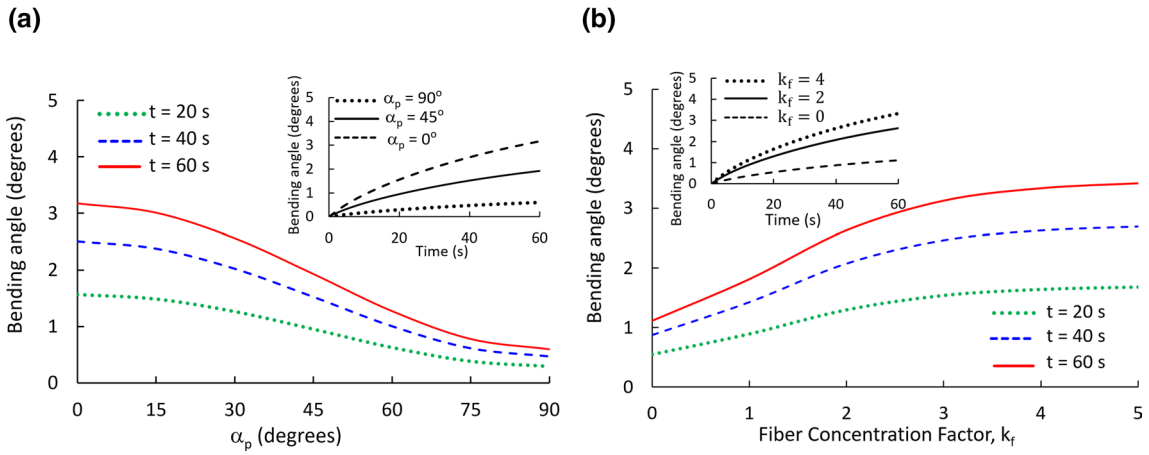

Fig. 7 The effects of **a** collagen fiber orientation α_p and **b** concentration factor k_f on the electroactive bending behavior of scleral strips. The numerical simulations were done using model parameters reported in Table 1 for experiments performed at 10 V

increasing the voltage and FCD. Figure 7 shows the effects of collagen fiber orientation and concentration factor on the bending angle of scleral strips. The critical role of collagen fibers in the biomechanical response of sclera has been previously confirmed (Coudrillier et al. 2015; Girard et al. 2011; Girard et al. 2009a). Here, scleral strips were cut in the superior–inferior direction from eyeballs near the equator line (Fig. 1). Figure 2 schematically shows meridional ($\alpha_p = 0°$) and circumferential ($\alpha_p = 90°$) fiber orientations. It should be noted that collagen fibers are meridionally aligned in the area close to the equator line (Girard et al. 2011). Thus, we used a preferred fiber orientation, i.e., $\alpha_p = 0°$, in numerical simulations, where the fibers were assumed to be confined within the yz-plane (Fig. 2b). We observed that changing the fiber orientation from the meridional into circumferential direction would significantly decrease the

scleral bending angle. The same trend could be seen with increasing the fiber concentration factor k_f. This parameter controls the collagen fiber alignment along a preferred fiber orientation and acts as an amplifying parameter on the bending response of scleral strips (Girard et al. 2009a). When k_f is equal to zero, collagen fibers are randomly oriented representing equal stiffness in all directions. On the other hand, if k_f becomes very large, fibers become perfectly oriented along the defined preferred orientation (Girard et al. 2009a). Figure 7 shows that increasing this parameter has a considerable effect on increasing the bending angle of the samples. This is an important numerical observation since collagen fibers have different orientation around the eyeball. Thus, we could hypothesize that strips obtained from different regions of eyeball would show different amount of bending deformation in response to an applied electric voltage.

This study has a number of limitations. For example, although numerical model parameters were in agreement with the range of values previously reported for monkey sclera (Feola et al. 2016; Girard et al. 2009b), a complete sensitivity analysis and using other optimization algorithms to obtain the fits can confirm their uniqueness (Hatami-Marbini and Maulik 2016). Furthermore, the current experiments can be complemented with mechanical experiments in order to obtain a better representation of numerical model parameters. For example, scleral strips prepared from the same region could be tested mechanically in order to have more experimental data for finding the material parameters. The numerical model was able to capture the experimental data, but there was some discrepancy between the model predictions and experimental results. This could be because of simplifications that we used in creating the numerical model as well as errors that may have happened during the experimental measurements. For example, using a semi-coupled scheme to solve required partial differential equations may have reduced the accuracy of the numerical model. We are currently working on a fully coupled solver for characterizing the electroactive response of the scleral tissue. In addition, we assumed that that pH waves propagating from the electrodes did not reach the samples during the experiments as it is shown in Fig. 3. The fixed charges inside the tissue are dependent on the pH of the surrounding medium (Elliott and Hodson 1998; Huang and Meek 1999; Loret and Simões 2010, 2017). We cannot refute minor changes to the pH of the solution near the samples. However, we expect that possible changes of the pH near the strips had little effects on experimental measurements. The proposed numerical model was not able to consider the effects of the pH gradient (e.g., penetration of pH waves inside the samples). We monitored the temperature of the solution using a thermometer (OMEGA—HH911T, CT, USA) and noticed that the temperature remained almost constant around 37 °C within the first three minutes of experiments performed under 15 V of electrical stimulation. The scleral mechanics depends on temperature; thus, the effect of temperature is another potential improvement that could be considered in future studies. All experiments were done in NaCl instead of pH buffered solutions; this was done to limit the number of ions in the solution and avoid unnecessary complications in the proposed numerical model. The pH buffered solutions include more than two ionic species, and Eq. (1) needs to be modified to be able to describe the concentration of different ions throughout the domain. We observed qualitatively similar electroactive response in PBS; however, the exact dependence of scleral electroactive response on solution composition and type requires more attention and will be investigated in our future studies. It is known that scleral collagen fibers have different orientation around the eyeball. However, we only obtained strips from the area close to the equator line and in the superior–inferior direction, i.e., we did not characterize the possible effects of fiber orientation experimentally. Despite this, the numerical model showed that the fiber orientation significantly affects the electromechanical response of the sclera, which can be experimentally verified by excising samples from other directions and from different parts of the eyeball in future studies. Finally, the numerical model was developed based on the assumption that the orientation of collagen fibers along the depth of the sclera is constant and there is no out-of-plane variation. However, collagen fibers are not solely distributed in plane (Gogola et al. 2018; Jan et al. 2017; Yang et al. 2018).

4 Summary and conclusions

In this paper, we used an experimental and numerical framework to investigate the electroactive response of sclera. For this purpose, we placed scleral strips in NaCl solution between two electrodes and recorded their bending deformation in an electric field. We observed that scleral strips bent toward cathode and the amount of their deformation was proportional to the magnitude of the applied DC voltage. Furthermore, we developed a computational CEM model to numerically represent the experimental measurements. In this model, we used the nonlinear coupled PNP system for the motion of charged ion species under the influence of the ionic concentration gradient and electric potential. Furthermore, we used a nonlinear anisotropic hyperelastic constitutive model for the mechanical response of sclera strips. The constitutive model was written as the summation of strain energies of the proteoglycan matrix domain and the collagen fiber reinforcements. We defined the coupling of chemo-electro-mechanical fields through the differential osmotic pressure. Using the numerical model, we studied the effect of a number of parameters, such as the magnitude of the electrical field, fixed charge density, and orientation

and concentration of collagen fibers on the deformation of scleral strips in an electric field.

The experimental and numerical framework of the present research can be used to estimate the amount of fixed charge density inside the tissue. This is because the electroactive response of the sclera is highly dependent on the fixed charge density. The GAG content of the sclera and subsequently the fixed charge density change in several eye-related disorders. For instance, the accumulation of GAGs has been reported as a possible factor in tumor extension in melanoma (Alyahya et al. 2003). In addition, the scleral GAG content is varied in eye diseases and disorders such as myopia and glaucoma (Murienne et al. 2015; Norton and Rada 1995). It is noted that the orientation of collagen fibers changes because of aging, glaucoma, and myopia (Coudrillier et al. 2015; Markov et al. 2018; Pijanka et al. 2012); a numerical model such as the one that was developed here is capable of separating the effects of collagen fiber orientation and fixed charge density. In such studies, the actual fiber distribution, instead of the theoretical fiber distributions considered here, can be fed into the numerical model. The amount of fixed charge density in the tissue can also be manipulated by removing GAGs enzymatically (Hatami-Marbini and Pachenari 2020c, 2021; Murienne et al. 2015). A better calibration of the numerical model parameters can be obtained by combining the electromechanical tests of the present work with the mechanical tests such as tensile experiments. It is noted that determining GAG density using chemical assays such as 1,9-dimethylmethylene blue (DMMB) assay makes the tissue inaccessible for any further analysis. However, the current methodology allows quantification of the GAG density without damaging the samples, i.e., mechanical properties of the samples can be determined after their electromechanical response has been characterized. The present work was focused on showing that sclera is an electroactive biomaterial and on developing a numerical framework for its electromechanical response. Future studies are required to extend the present study and show its application for better understanding the mechanical behavior of sclera.

Appendix 1: Validation of hyperelastic mechanical model

We verified the FE implementation of the proposed nonlinear hyperelastic behavior model by performing a numerical biaxial extension test on a hexahedron element and comparing it to the analytical solution. The model parameters were $c_1 = 10$ Pa, $c_3 = 50$ Pa, $c_4 = 5$, and $K = 1$ MPa. We assumed that all fibers were contained within the xy-plane and in the y-direction. We considered different values for the fiber concentration factor k_f. Figure 8 shows that there is an excellent agreement between the numerical and analytical values. In addition, our numerical results agree with previous studies (Girard et al. 2009a).

Appendix 2: Validation of chemo-electro-mechanical model

We validated the numerical implementation of the CEM model of the present study by solving a special case where linear elastic constitutive equations are considered for the mechanical field and solved previously by Wallmersperger

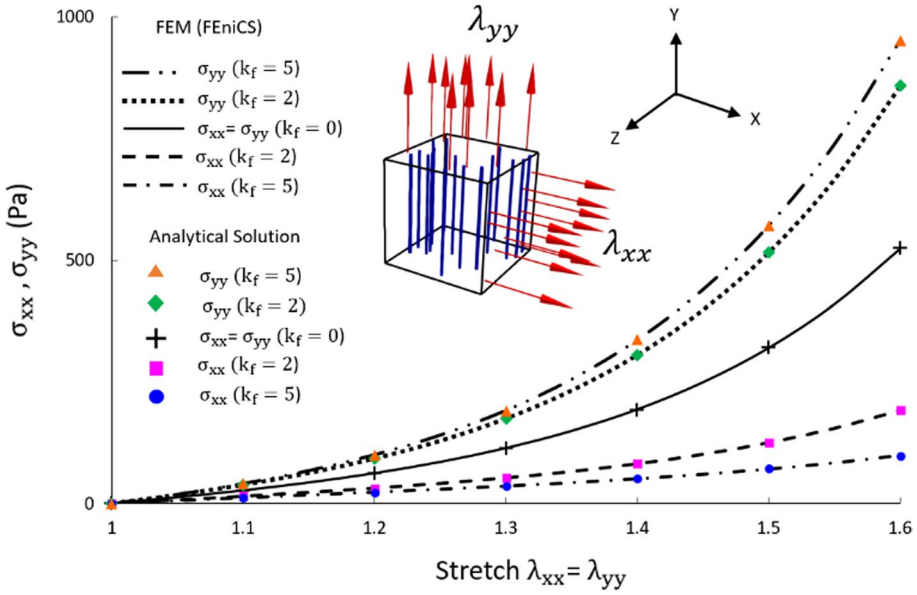

Fig. 8 Validation of the nonlinear hyperelastic model for the biaxial extension test on a hexahedral element. The inset figure shows the element where the blue bars inside the cube indicate the fibers that are aligned in the y-direction. It is seen that σ_{yy} increases, while σ_{xx} decreases with increasing k_f

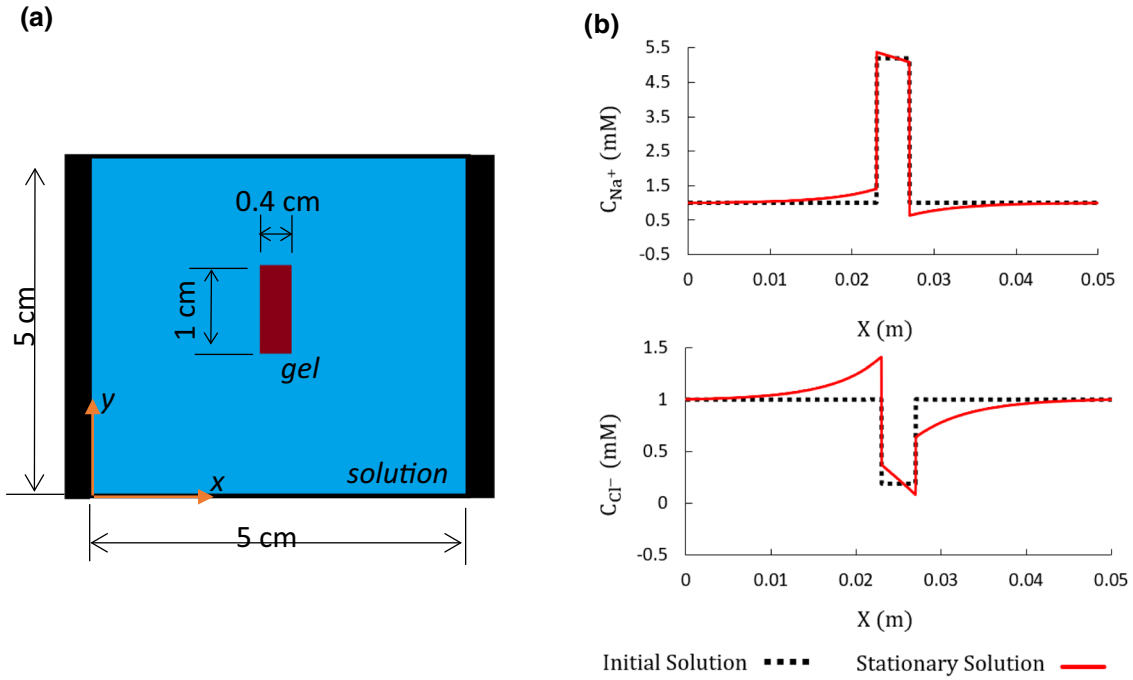

Fig. 9 **a** A rectangular gel in a solution bath subjected to an electric field. **b** The initial (dashed lines) and stationary (solid lines) concentrations of sodium and chloride ions at $y = 0.025$ m

Table 2 Parameters used for solving the PNP system (Wallmersperger et al. 2004)

Parameter	F	ε_0	ε_r	z_{Na}	z_{Cl}	z_{fixed}	R	T	D_{Na^+}	D_{Cl^-}
Value	96,487	8.85×10^{-12}	100	1	−1	−1	8.3114	293	10^{-7}	10^{-7}
Unit	c/mol	F/m					J/mol K	K	m^2/s	m^2/s

Table 3 Initial and boundary conditions (Wallmersperger et al. 2004)

Initial conditions		Boundary conditions	
Solution	Gel	Anode	Cathode
$C_{Na^+} = 1$ mM	$C_{Na^+} = 5.193$ mM	$\phi = 0.1$ V	$\phi = -0.1$ V
$C_{Cl^-} = 1$ mM	$C_{Cl^-} = 0.193$ mM	$C_{Na^+} = 1$ mM	$C_{Na^+} = 1$ mM
	$C_{fixed} = 5$ mM	$C_{Cl^-} = 1$ mM	$C_{Cl^-} = 1$ mM

et al. (2004). To this end, we considered a 5 cm × 5 cm solution domain with a 4 mm × 10 mm rectangular gel domain at the center (Fig. 9). The parameters used in this simulation along with the initial and boundary conditions are given in Tables 2, and 3 and are the same as those used in the previous study (Wallmersperger et al. 2004). The distribution of sodium and chloride ions is plotted in Fig. 9. An excellent agreement is observed between the results shown in Fig. 9 and those previously published.

Acknowledgements The authors would like to acknowledge the support in part by National Science Foundation: Grant No. 1635290.

Declarations

Conflict of interest The authors declare that they have no conflict of interest to report.

References

Alnæs M et al (2015) The FEniCS project version 1.5. Archive of Numerical Software 3

Alyahya GA, Ribel-Madsen SM, Heegaard S, Prause JU, Trier K (2003) Melanoma-associated spongiform scleropathy: biochemical changes and possible relation to tumour extension. Acta Ophthalmol Scand 81:625–629

Attaran A, Brummund J, Wallmersperger T (2015) Modeling and simulation of the bending behavior of electrically-stimulated cantilevered hydrogels. Smart Mater Struct 24:035021

Attaran A, Keller K, Wallmersperger T (2018) Modeling and simulation of hydrogels for the application as finger grippers. J Intell Mater Syst Struct 29:371–387

Ballhause D, Wallmersperger T (2008) Coupled chemo-electro-mechanical finite element simulation of hydrogels: I. Chem Stimul Smart Mater Struct 17:045011

Bassetti MJ, Chatterjee AN, Aluru NR, Beebe DJ (2005) Development and modeling of electrically triggered hydrogels for microfluidic applications. J Microelectromech Syst 14:1198–1207

Bassil M, Ibrahim M, El Tahchi M (2011) Artificial muscular microfibers: hydrogel with high speed tunable electroactivity. Soft Matter 7:4833–4838

Boote C, Sigal IA, Grytz R, Hua Y, Nguyen TD, Girard MJA (2020) Scleral structure and biomechanics. Prog Retin Eye Res 74:100773

Borcherding MS, Blacik L, Sittig R, Bizzell JW, Breen M, Weinstein H (1975) Proteoglycans and collagen fibre organization in human corneoscleral tissue. Exp Eye Res 21:59–70

Bradski G, Kaehler A (2008) Learning OpenCV: computer vision with the OpenCV library. O'Reilly Media Inc.

Chen S, Birk DE (2013) The regulatory roles of small leucine-rich proteoglycans in extracellular matrix assembly. FEBS J 280:2120–2137

Chen J, Ma G (2006) Modelling deformation behaviour of polyelectrolyte gels under chemo-electro-mechanical coupling effects. Int J Numer Methods Eng 68:1052–1071

Cheng X, Hatami-Marbini H, Pinsky PM (2013) Modeling collagen-proteoglycan structural interactions in the human cornea. In: Computer models in biomechanics. Springer, pp 11–24

Chen D et al (2020) Distinct effects of different matrix proteoglycans on collagen fibrillogenesis and cell-mediated collagen reorganization. Sci Rep 10:19065

Chinthala VSRK, Mulay SS, Harish AB (2021) Constitutive modeling of pH-sensitive hydrogel: multi-physics coupling of electromagnetics with mechanics and thermodynamics. Mech Mater 161:104002

Coudrillier B, Pijanka J, Jefferys J, Sorensen T, Quigley HA, Boote C, Nguyen TD (2015) Collagen structure and mechanical properties of the human sclera: analysis for the effects of age. J Biomech Eng 137:041006

De SK, Aluru NR (2004) A chemo-electro-mechanical mathematical model for simulation of pH sensitive hydrogels. Mech Mater 36:395–410

De SK, Aluru N, Johnson B, Crone W, Beebe DJ, Moore J (2002) Equilibrium swelling and kinetics of pH-responsive hydrogels: models, experiments, and simulations. J Microelectromech Syst 11:544–555

De Gennes P, Okumura K, Shahinpoor M, Kim KJ (2000) Mechanoelectric effects in ionic gels. EPL (europhysics Letters) 50:513

Doi M, Matsumoto M, Hirose Y (1992) Deformation of ionic polymer gels by electric fields. Macromolecules 25:5504–5511

Elliott GF, Hodson SA (1998) Cornea, and the swelling of polyelectrolyte gels of biological interest. Rep Prog Phys 61:1325

Elshaer S, Moussa W (2014) Comparative study of chemo-electro-mechanical transport models for an electrically stimulated hydrogel. Smart Mater Struct 23:075022

Farooqi AR, Zimmermann J, Bader R, van Rienen U (2020) Computational study on electromechanics of electroactive hydrogels for cartilage-tissue repair. Comput Methods Progr Biomed 197:105739

Feola AJ, Myers JG, Raykin J, Mulugeta L, Nelson ES, Samuels BC, Ethier CR (2016) Finite element modeling of factors influencing optic nerve head deformation due to intracranial pressure. IOVS 57:1901–1911

Flory PJ, Rehner JJ (1943a) Statistical mechanics of cross-linked polymer networks I. Rubberlike Elast J Chem Phys 11:512–520

Flory PJ, Rehner JJ (1943b) Statistical mechanics of cross-linked polymer networks II. Swelling J Chem Phys 11:521–526

Forrester JV, Dick AD, McMenamin P, Lee W (1996) The eye basic sciences in practice. Elsevier

Gandhi NS, Mancera RL (2008) The structure of glycosaminoglycans and their interactions with proteins. Chem Biol Drug Des 72:455–482

Girard MJ, Downs JC, Burgoyne CF, Suh J-KF (2009a) Peripapillary and posterior scleral mechanics—part I: development of an anisotropic hyperelastic constitutive model. J Biomech Eng 131:051011

Girard MJ, Suh JK, Bottlang M, Burgoyne CF, Downs JC (2009b) Scleral biomechanics in the aging monkey eye. Invest Ophthalmol vis Sci 50:5226–5237

Girard MJ et al (2011) Quantitative mapping of scleral fiber orientation in normal rat eyes. Investig Ophthalmol vis Sci 52:9684–9693

Glazer P, Van Erp M, Embrechts A, Lemay S, Mendes E (2012) Role of pH gradients in the actuation of electro-responsive polyelectrolyte gels. Soft Matter 8:4421–4426

Gogola A, Jan N-J, Lathrop KL, Sigal IA (2018) Radial and circumferential collagen fibers are a feature of the peripapillary sclera of human, monkey, pig, cow, goat, and sheep. Investig Ophthalmol vis Sci 59:4763–4774

Gong J, Nitta T, Osada Y (1994) Electrokinetic modeling of the contractile phenomena of polyelectrolyte gels. One-Dimens Capill Model J Phys Chem 98:9583–9587

Grimshaw P, Nussbaum J, Grodzinsky A, Yarmush M (1990) Kinetics of electrically and chemically induced swelling in polyelectrolyte gels. J Chem Phys 93:4462–4472

Grytz R, Meschke G (2009) Constitutive modeling of crimped collagen fibrils in soft tissues. J Mech Behav Biomed Mater 2:522–533

Gu WY, Yao H, Vega AL, Flagler D (2004) Diffusivity of ions in agarose gels and intervertebral disc: effect of porosity. Ann Biomed Eng 32:1710–1717

Guelch RW, Holdenried J, Weible A, Wallmersperger T, Kroeplin B Polyelectrolyte gels in electric fields: a theoretical and experimental approach. In: Smart structures and materials 2000: electroactive polymer actuators and devices (EAPAD), 2000. International Society for Optics and Photonics, pp 193–202

Hatami-Marbini H (2013) Mechano-electrochemical mixture theories for the multiphase fluid infiltrated poroelastic media. In: Li S, Gao X-L (eds) Handbook on micromechanics and nanomechanics. Pan Stanford Publishing Pte. Ltd, pp 273–302

Hatami-Marbini H (2014) Hydration dependent viscoelastic tensile behavior of cornea. Ann Biomed Eng 42:1740–1748

Hatami-Marbini H, Etebu E (2013) Hydration dependent biomechanical properties of the corneal stroma. Exp Eye Res 116:47–54

Hatami-Marbini H, Maulik R (2016) A biphasic transversely isotropic poroviscoelastic model for the unconfined compression of hydrated soft tissue. J Biomech Eng 138:031003

Hatami-Marbini H, Pachenari M (2020a) The contribution of sGAGs to stress-controlled tensile response of posterior porcine sclera. PLoS ONE 15:e0227856

Hatami-Marbini H, Pachenari M (2020b) Hydration related changes in tensile response of posterior porcine sclera. J Mech Behav Biomed Mater 104:103562

Hatami-Marbini H, Pachenari M (2020c) On influence of sulfated glycosaminoglycans on tensile properties of posterior sclera. Mech Soft Mater 2:1–10

Hatami-Marbini H, Pachenari M (2021) Tensile viscoelastic properties of the sclera after glycosaminoglycan depletion. Curr Eye Res 46:1–10

Hatami-Marbini H, Pinsky PM (2009) On mechanics of connective tissue: assessing the electrostatic contribution to corneal stroma elasticity. In: MRS online proceedings library (OPL), vol 1239

Hatami-Marbini H, Etebu E, Rahimi A (2013) Swelling pressure and hydration behavior of porcine corneal stroma. Curr Eye Res 38:1124–1132

Holzapfel AG (2000) Nonlinear solid mechanics: a continuum approach for engineering. Wiley

Huang Y, Meek KM (1999) Swelling studies on the cornea and sclera: the effects of pH and ionic strength. Biophys J 77:1655–1665

Jan N-J, Lathrop K, Sigal IA (2017) Collagen architecture of the posterior pole: high-resolution wide field of view visualization and analysis using polarized light microscopy. IOVS 58:735–744

Jiang H, Fan L, Yan S, Li F, Li H, Tang J (2019) Tough and electro-responsive hydrogel actuators with bidirectional bending behavior. Nanoscale 11:2231–2237

Kim SY, Shin HS, Lee YM, Jeong CN (1999) Properties of electroresponsive poly (vinyl alcohol)/poly (acrylic acid) IPN hydrogels under an electric stimulus. J Appl Polym Sci 73:1675–1683

Kwon IC, Bae YH, Kim SW (1994) Characteristics of charged networks under an electric stimulus. J Polym Sci B Polym Phys 32:1085–1092

Langtangen HP, Mardal K-A (2016) Introduction to numerical methods for variational problems. Springer

Lanir Y, Seybold J, Schneiderman R, Huyghe J (1998) Partition and diffusion of sodium and chloride ions in soft charged foam: the effect of external salt concentration and mechanical deformation. Tissue Eng 4:365–378

Lewis PN, Pinali C, Young RD, Meek KM, Quantock AJ, Knupp C (2010) Structural interactions between collagen and proteoglycans are elucidated by three-dimensional electron tomography of bovine cornea. Structure 18:239–245

Li H, Lai F (2011) Transient analysis of the effect of the initial fixed charge density on the kinetic characteristics of the ionic-strength-sensitive hydrogel by a multi-effect-coupling model. Anal Bioanal Chem 399:1233–1243

Li H, Yuan Z, Lam K, Lee H, Chen J, Hanes J, Fu J (2004) Model development and numerical simulation of electric-stimulus-responsive hydrogels subject to an externally applied electric field. Biosens Bioelectron 19:1097–1107

Li Y, Sun Y, Xiao Y, Gao G, Liu S, Zhang J, Fu J (2016) Electric field actuation of tough electroactive hydrogels cross-linked by functional triblock copolymer micelles. ACS Appl Mater Interfaces 8:26326–26331

Liu W, Collins CM, Smith MB (2005) Calculations of B(1) distribution, specific energy absorption rate, and intrinsic signal-to-noise ratio for a body-size birdcage coil loaded with different human subjects at 64 and 128 MHz. Appl Magn Reson 29:5–18

Logg A, Mardal K-A, Wells G (2012) Automated solution of differential equations by the finite element method: the FEniCS book, vol 84. Springer, Berlin

Loret B, Simões FM (2010) Effects of pH on transport properties of articular cartilages. Biomech Model Mechanobiol 9:45–63

Loret B, Simões FM (2017) Biomechanical aspects of soft tissues. CRC Press, Boca Raton

Luo R, Li H, Lam K (2007) Coupled chemo-electro-mechanical simulation for smart hydrogels that are responsive to an external electric field. Smart Mater Struct 16:1185

Markov PP et al (2018) Bulk changes in posterior scleral collagen microstructure in human high myopia. Mol vis 24:818

Meek KM (2008) The cornea and sclera. In: Fratzl P (ed) Collagen: structure and mechanics. Springer US, Boston, pp 359–396

Mehr JA, Hatami-Marbini H (2022) Experimental and numerical analysis of electroactive characteristics of scleral tissue. Acta Biomater 143:127–137

Morales D, Palleau E, Dickey MD, Velev OD (2014) Electro-actuated hydrogel walkers with dual responsive legs. Soft Matter 10:1337–1348

Murienne BJ, Jefferys JL, Quigley HA, Nguyen TD (2015) The effects of glycosaminoglycan degradation on the mechanical behavior of the posterior porcine sclera. Acta Biomater 12:195–206

Norton TT, Rada JA (1995) Reduced extracellular matrix in mammalian sclera with induced myopia. Vis Res 35:1271–1281

O'Grady ML, Kuo P-L, Parker KK (2009) Optimization of electroactive hydrogel actuators. ACS Appl Mater Interfaces 2:343–346

Pachenari M, Hatami-Marbini H (2021) Regional differences in the glycosaminoglycan role in porcine scleral hydration and mechanical behavior. IOVS 62:28–28

Pijanka JK et al (2012) Quantitative mapping of collagen fiber orientation in non-glaucoma and glaucoma posterior human sclerae. Investig Ophthalmol vis Sci 53:5258–5270

Pomin VH, Mulloy B (2018) Glycosaminoglycans and proteoglycans. Pharmaceuticals (basel) 11:27

Price K, Storn RM, Lampinen JA (2006) Differential evolution: a practical approach to global optimization. Springer

Rada JA, Achen VR, Perry CA, Fox PW (1997) Proteoglycans in the human sclera. Evidence for the presence of aggrecan. IOVS 38:1740–1751

Scott JE, Thomlinson AM (1998) The structure of interfibrillar proteoglycan bridges (shape modules') in extracellular matrix of fibrous connective tissues and their stability in various chemical environments. J Anat 192(Pt 3):391–405

Shang J, Shao Z, Chen X (2008a) Chitosan-based electroactive hydrogel. Polymer 49:5520–5525

Shang J, Shao Z, Chen X (2008b) Electrical behavior of a natural polyelectrolyte hydrogel: chitosan/carboxymethylcellulose hydrogel. Biomacromol 9:1208–1213

Shiga T, Kurauchi T (1990) Deformation of polyelectrolyte gels under the influence of electric field. J Appl Polym Sci 39:2305–2320

Sun S, Mak AF (2001) The dynamical response of a hydrogel fiber to electrochemical stimulation. J Polym Sci B Polym Phys 39:236–246

Vogel KG, Trotter JA (1987) The effect of proteoglycans on the morphology of collagen fibrils formed in vitro. Collagen Relat Res 7:105–114

Wallmersperger T, Kröplin B, Gülch RW (2004) Coupled chemo-electro-mechanical formulation for ionic polymer gels—numerical and experimental investigations. Mech Mater 36:411–420

Wallmersperger T, Ballhause D, Kröplin B (2007) On the modeling of polyelectrolyte gels. In: Macromolecular symposia, vol 1. Wiley Online Library, pp 306–313

Wallmersperger T, Attaran A, Keller K, Brummund J, Guenther M, Gerlach G (2013) Modeling and simulation of hydrogels for the application as bending actuators. In: Sadowski G, Richtering W (eds) Intelligent hydrogels. Springer International Publishing, Cham, pp 189–204

Wang S, Hatami-Marbini H (2021) Constitutive modeling of corneal tissue: influence of three-dimensional collagen fiber microstructure. J Biomech Eng 143:031002

Weiss JA, Maker BN, Govindjee S (1996) Finite element implementation of incompressible, transversely isotropic hyperelasticity. Comput Methods Appl Mech Eng 135:107–128

Yang B, Brazile B, Jan N-J, Hua Y, Wei J, Sigal IA (2018) Structured polarized light microscopy for collagen fiber structure and orientation quantification in thick ocular tissues. J Biomed Opt 23:106001

Yew Y, Ng T, Li H, Lam K (2007) Analysis of pH and electrically controlled swelling of hydrogel-based micro-sensors/actuators. Biomed Microdevices 9:487–499

Yuan Z, Li H (2013) Modeling development and numerical simulation of transient nonlinear behaviors of electric-sensitive hydrogel membrane under an external electric field. J Biochip Tissue Chip 3:1–13

Zhang F, Zhang Z, Linhardt RJ (2010) Chapter 3—Glycosaminoglycans. In: Cummings RD, Pierce JM (eds) Handbook of glycomics. Academic Press, San Diego, pp 59–80

Zhang Y-F et al (2020) Supramolecular ionic polymer/carbon nanotube composite hydrogels with enhanced electromechanical performance. Nanotechnol Rev 9:478–488